Longitudinal and Transverse $^1H-^{15}N$ Dipolar/^{15}N Chemical Shift Anisotropy Relaxation Interference: Unambiguous Determination of Rotational Diffusion Tensors and Chemical Exchange Effects in Biological Macromolecules

Christopher D. Kroenke,† J. Patrick Loria,† Larry K. Lee,† Mark Rance,*,‡ and Arthur G. Palmer, III*,†

Contribution from the Department of Biochemistry and Molecular Biophysics, Columbia University, 630 West 168th Street, New York, New York 10032, and Department of Molecular Genetics, Biochemistry, and Microbiology, University of Cincinnati, Cincinnati, Ohio 45267

Received March 12, 1998

Abstract: High-resolution proton-detected heteronuclear correlation NMR spectroscopy allows the measurement of ^{15}N spin relaxation rates at multiple sites throughout a biological macromolecule. The rate constants are determined by stochastic internal motions on time scales of picoseconds to nanoseconds, overall molecular rotational diffusion on time scales of nanoseconds, and chemical exchange rates on time scales of microseconds to milliseconds. A new method has been developed for distinguishing the contributions of chemical exchange from the contributions due to anisotropic rotational diffusion by measuring both longitudinal and transverse interference between the $^1H-^{15}N$ dipolar and ^{15}N chemical shift anisotropy interactions. The spectroscopic experiment for measuring the longitudinal cross-correlation rate constant for $^1H-^{15}N$ dipolar/^{15}N chemical shift anisotropy interference is based on the approach for measuring the transverse cross-correlation rate constant (Tjandra, N.; Szabo, A.; Bax, A. *J. Am. Chem. Soc.* **1996**, *118*, 6986−6991) but incorporates a novel method for averaging the relaxation rates of longitudinal magnetization and two spin order. Application of this technique to *Escherichia coli* ribonuclease H affords an improved description of rotational diffusion anisotropy and permits a more accurate assessment of chemical exchange in this molecule. The results definitively demonstrate that amino acid residues K60 and W90 are subject to conformational exchange processes, whereas increased transverse relaxation rates for residues in the helix α_D arise from anisotropic rotational diffusion.

Introduction

Nuclear magnetic spin relaxation rates of ^{15}N nuclei provide sensitive probes of the dynamic behavior of proteins and nucleic acids in solution.[1,2] In the usual protocol, the ^{15}N longitudinal relaxation rate constant (R_1), the ^{15}N transverse relaxation rate constant (R_2), and the $^1H-^{15}N$ heteronuclear cross relaxation rate constant (σ_{NH}) are measured, at one or more static magnetic field strengths, for a large number of atomic sites within a macromolecule using two-dimensional proton-detected heteronuclear correlation NMR spectroscopy.[3] The relaxation parameters are analyzed using the reduced spectral density mapping[4−7] and model-free formalisms.[8−10] The R_1, R_2, and σ_{NH} relaxation rate constants are determined principally by the $^1H-^{15}N$ dipolar and ^{15}N chemical shift anisotropy (CSA) relaxation mechanisms; however, the R_2 relaxation rate constant may contain additional contributions from chemical or conformational kinetic processes that exchange an ^{15}N nucleus between multiple sites characterized by different chemical shifts. Significant exchange contributions to transverse relaxation are observed for kinetic processes on microsecond to millisecond time scales in biological macromolecules.[11−14]

Accurate assessment of chemical exchange contributions to R_2 is critical for a proper interpretation of both model-free and spectral density mapping results. If a biological macromolecule is regarded as a spherical top that rotates isotropically in solution, then the trimmed mean value of the ratio R_2/R_1 provides an estimate of the isotropic rotational correlation time of the molecule.[3] Atomic sites subject to large amplitude motions on time scales faster than rotational diffusion yield significantly smaller R_2/R_1 ratios (and reduced values of the heteronuclear $\{^1H\}^{15}N$ nuclear Overhauser effect (NOE)). Atomic sites subject to chemical or conformational exchange have signifi-

* To whom correspondence should be addressed. E-mail: rance@rabi.med.uc.edu (M.R.) or agp6@columbia.edu (A.G.P.).
† Columbia University.
‡ University of Cincinnati.

(1) Palmer, A. G.; Williams, J.; McDermott, A. *J. Phys. Chem.* **1996**, *100*, 13293−13310.
(2) Palmer, A. G. *Curr. Opin. Struct. Biol.* **1997**, *7*, 732−737.
(3) Kay, L. E.; Torchia, D. A.; Bax, A. *Biochemistry* **1989**, *28*, 8972−8979.
(4) Farrow, N. A.; Zhang, O.; Szabo, A.; Torchia, D. A.; Kay, L. E. *J. Biomol. NMR* **1995**, *6*, 153−162.
(5) Ishima, R.; Nagayama, K. *J. Magn. Reson., Ser. B* **1995**, *108*, 73−76.
(6) Peng, J.; Wagner, G. *Biochemistry* **1995**, *34*, 16733−16752.
(7) Lefèvre, J. F.; Dayie, K. T.; Peng, J. W.; Wagner, G. *Biochemistry* **1996**, *35*, 2674−2686.
(8) Halle, B.; Wennerström, H. *J. Chem. Phys.* **1981**, *75*, 1928−1943.
(9) Lipari, G.; Szabo, A. *J. Am. Chem. Soc.* **1982**, *104*, 4559−4570.
(10) Lipari, G.; Szabo, A. *J. Am. Chem. Soc.* **1982**, *104*, 4546−4559.
(11) Clore, G. M.; Driscoll, P. C.; Wingfield, P. T.; Gronenborn, A. M. *Biochemistry* **1990**, *29*, 7387−7401.
(12) Szyperski, T.; Luginbühl, P.; Otting, G.; Güntert, P.; Wüthrich, K. *J. Biomol. NMR* **1993**, *3*, 151−164.
(13) Orekhov, V. Y.; Pervushin, K. V.; Arseniev, A. S. *Eur. J. Biochem.* **1994**, *219*, 887−896.
(14) Akke, M.; Liu, J.; Cavanagh, J.; Erickson, H. P.; Palmer, A. G. *Nat. Struct. Biol.* **1998**, *5*, 55−59.

S0002-7863(98)00832-4 CCC: $15.00
Published on Web 07/21/1998

cantly larger R_2/R_1 ratios.[11,15] A large number of studies of backbone amide ^{15}N spin relaxation in proteins have been reported in which intramolecular dynamic properties have been analyzed using the model-free formalism under the assumption that rotational diffusion can be described using a single rotational correlation time.[2]

A serious complication arises if the rotational diffusion of the molecule is not isotropic. Anisotropic overall rotation was anticipated in the original work of Lipari and Szabo[9,10] and Halle and Wennerström.[8] Several groups have subsequently interpreted experimental ^{15}N spin relaxation data using an anisotropic diffusion tensor.[15−21] If rotational diffusion anisotropy is significant, increases in the values of R_2/R_1 for an ^{15}N spin can result from particular orientations of the symmetry axis of the dipolar or CSA tensor in the principal axis frame of the diffusion tensor. These increases can be interpreted mistakenly as evidence of conformational exchange.[22] At the same time, real chemical exchange contributions to R_2 interfere with measurements of the rotational diffusion anisotropy by systematically increasing the R_2/R_1 ratios for the affected spins. In practice, sites with large R_2/R_1 ratios are excluded from analysis,[15] which reduces the available data and risks exclusion of data important for accurate assessment of rotational diffusion anisotropy.[20]

Conformational exchange can be identified by measuring the dependence of the relaxation rates on the static magnetic field strength; however, a wide range of fields is necessary to accurately separate the field dependence of chemical exchange and CSA.[4,6,23] Conformational exchange also can be identified, and kinetic processes characterized quantitatively, by rotating frame spin relaxation measurements;[24] however, relatively few of these studies have focused on biological macromolecules.[12−14,25] Tjandra et al. reported a method for measuring the transverse cross-correlation relaxation rate constant (η_{xy}) that results from interference between the ^{1}H−^{15}N dipolar and ^{15}N CSA interactions and noted that this relaxation rate mechanism is independent of chemical exchange effects.[26] Although this experiment potentially provides a means of identifying chemical exchange,[27] in practice, the principal values and orientation of the ^{15}N CSA tensor are not known accurately enough to interpret η_{xy} quantitatively in terms of molecular motions. For example, the principal values of ^{15}N CSA tensors determined in model compounds by solid-state NMR spectroscopy vary by ±10%.[28−30]

Herein, we present a method for measuring longitudinal cross-correlation relaxation rate constants (η_z) for ^{1}H−^{15}N dipolar/^{15}N CSA relaxation interference in biological macromolecules. Both η_{xy} and η_z are independent of chemical exchange and the η_{xy}/η_z ratio is, to a good approximation, independent of the principal values and orientations of the CSA tensor. Consequently, the η_{xy}/η_z ratio is sensitive only to internal and overall motions that contribute to dipolar and CSA relaxation mechanisms. The dependence of the η_{xy}/η_z ratio on the orientation of the H−N bond vector in a molecular reference frame provides a robust method of determining the rotational diffusion tensor. Furthermore, comparison of the η_{xy}/η_z ratios to the R_2/R_1 ratios measured at a single static magnetic field strength permits unequivocal identification of ^{15}N nuclei that are subject to chemical exchange processes. Theoretical and experimental aspects of this method are outlined in the following sections. For simplicity, only the backbone amide group in polypeptides is considered; however, similar theoretical and experimental methods are applicable to relaxation studies of imino groups in nucleic acids.[31] The new method is applied to ^{2}H/^{15}N-labeled *Escherichia coli* ribonuclease H (RNaseH), a small (155 amino acid residues, $M_r = 17.6$ kD) protein whose dynamic properties have been extensively studied by NMR spectroscopy.[32−34] Combined use of both longitudinal and transverse relaxation interference measurements provides substantially better assessment of rotational diffusion anisotropy and demonstrates that a number of chemical exchange effects previously identified in RNaseH[32,34] resulted from underestimation of the anisotropy of the rotational diffusion tensor determined from R_2/R_1 ratios.

Theory

The theoretical exegesis follows closely the presentation of Goldman.[35] The spin operators for the ^{15}N nucleus will be denoted S_ζ and the spin operators for the ^{1}H nucleus will be denoted I_ζ, in which $\zeta = x$, y, or z. The symbol $\langle A\rangle(t)$ will be used to denote the operation Trace$\{\mathbf{A}\sigma(t)\}$ in which $\mathbf{A}$ is a basis operator and $\sigma(t)$ is the density operator.

An amide ^{15}N spin in a polypeptide backbone has a chemical shift tensor that can be approximated as axially symmetric with a width of approximately −160 ppm.[28−30] At magnetic fields typically employed in NMR studies of biological macromolecules, relaxation of ^{15}N spins has significant contributions from both the ^{1}H−^{15}N dipolar interaction with the covalently attached amide proton and the ^{15}N CSA interaction with the static magnetic field. The angle β between the symmetry axis of the ^{15}N CSA tensor and the ^{15}N−^{1}H bond vector is estimated to be less than 20° for a peptide backbone amide group,[28−30] and to a good approximation $J^{\mathrm{Dipolar}}(\omega) \approx J^{\mathrm{CSA}}(\omega) = J(\omega)$, where $J(\omega)$, the power spectral density function, describes the frequency distribution of stochastic motions that modulate the dipolar and CSA Hamiltonians,[26,36] and is given by

(15) Tjandra, N.; Feller, S. E.; Pastor, R. W.; Bax, A. *J. Am. Chem. Soc.* **1995**, *117*, 12562−12566.
(16) Schurr, J. M.; Babcock, H. P.; Fujimoto, B. S. *J. Magn. Reson., Ser. B* **1994**, *105*, 211−224.
(17) Zink, T.; Ross, A.; Lüers, K.; Cieslar, C.; Rudolph, R.; Holak, T. A. *Biochemistry* **1994**, *33*, 8453−8463.
(18) Brüschweiler, R.; Liao, X.; Wright, P. E. *Science* **1995**, *268*, 886−889.
(19) Zheng, Z.; Czaplicki, J.; Jardetzky, O. *Biochemistry* **1995**, *34*, 5212−5223.
(20) Lee, L. K.; Rance, M.; Chazin, W. J.; Palmer, A. G. *J. Biomol. NMR* **1997**, *9*, 287−298.
(21) Luginbühl, P.; Pervushin, K. V.; Iwai, H.; Wüthrich, K. *Biochemistry* **1997**, *36*, 7305−7312.
(22) Tjandra, N.; Wingfield, P.; Stahl, S.; Bax, A. *J. Biomol. NMR* **1996**, *8*, 273−284.
(23) Phan, I. Q. H.; Boyd, J.; Campbell, I. D. *J. Biomol. NMR* **1996**, *8*, 369−378.
(24) Deverell, C.; Morgan, R. E.; Strange, J. H. *Mol. Phys.* **1970**, *18*, 553−559.
(25) Zinn-Justin, S.; Berthault, P.; Guenneugues, M.; Desvaux, H. *J. Biomol. NMR* **1997**, *10*, 363−372.
(26) Tjandra, N.; Szabo, A.; Bax, A. *J. Am. Chem. Soc.* **1996**, *118*, 6986−6991.
(27) Brutscher, B.; Brüschweiler, R.; Ernst, R. R. *Biochemistry* **1997**, *36*, 13043−13053.
(28) Oas, T. G.; Hartzell, C. J.; Dahlquist, F. W.; Drobny, G. P. *J. Am. Chem. Soc.* **1987**, *109*, 5962−5966.
(29) Hiyama, Y.; Niu, C.-H.; Silverton, J. V.; Bavoso, A.; Torchia, D. A. *J. Am. Chem. Soc.* **1988**, *110*, 2378−2383.
(30) Shoji, A.; Ozaki, T.; Fujito, T.; Deguchi, K.; Ando, S.; Ando, I. *J. Am. Chem. Soc.* **1990**, *112*, 4693−4697.
(31) Akke, M.; Fiala, R.; Jiang, F.; Patel, D.; Palmer, A. G. *RNA* **1997**, *3*, 702−709.
(32) Mandel, A. M.; Akke, M.; Palmer, A. G. *J. Mol. Biol.* **1995**, *246*, 144−163.
(33) Yamasaki, K.; Saito, M.; Oobatake, M.; Kanaya, S. *Biochemistry* **1995**, *34*, 6587−6601.
(34) Mandel, A. M.; Akke, M.; Palmer, A. G. *Biochemistry* **1996**, *35*, 16009−16023.
(35) Goldman, M. *J. Magn. Reson.* **1984**, *60*, 437−452.
(36) Abragam, A. *Principles of Nuclear Magnetism*; Clarendon Press: Oxford, U.K., 1961.

$$J(\omega) = {}^2/_5\sum_{k=1}^{3} A_k\{S^2\tau_k/(1+\omega^2\tau_k{}^2) + (1-S^2)\tau'_k/(1+\omega^2\tau'^2_k)\} \quad (1)$$

in which $A_1 = (3\cos^2\theta - 1)^2/4$, $A_2 = 3\sin^2\theta\cos^2\theta$, $A_3 = ({}^3/_4)\sin^4\theta$, $\tau_1 = (6D_\perp)^{-1}$, $\tau_2 = (D_\parallel + 5D_\perp)^{-1}$, $\tau_3 = (4D_\parallel + 2D_\perp)^{-1}$, $\tau'_k = (\tau_k\tau_e)/(\tau_k + \tau_e)$, S^2 is the square of the generalized order parameter, τ_e is the effective correlation time for internal motions, $D_\parallel$ and $D_\perp$ are the rotational diffusion constants parallel and perpendicular to the symmetry axis of an axially symmetric rotational diffusion tensor, and θ is the angle between the symmetry axis of the diffusion tensor and the H−N bond vector.[16,37,38]

Because both the ^{1}H−^{15}N dipolar and ^{15}N CSA Hamiltonians transform as second rank tensors, cross-correlation, or interference, between dipolar and CSA interactions contributes to both relaxation[35] and dynamic frequency shifts.[39] The asymmetry of the ^{1}H−^{15}N scalar-coupled multiplet results from this interference and can be represented as a cross-correlation rate constant η_{xy} for cross-relaxation between in-phase magnetization, S_x (or S_y), and antiphase coherence, $2I_zS_x$ (or $2I_zS_y$). The same interference results in cross-relaxation between S_z longitudinal magnetization and two spin order, $2I_zS_z$, with cross-correlation rate constant η_z. As a consequence, the population difference between the $|\alpha\alpha>$ and $|\alpha\beta>$ states relaxes toward equilibrium at a different rate than the population difference between the $|\beta\alpha>$ and $|\beta\beta>$ states. The theoretical expressions for the cross-correlation rate constants are[35]

$$\eta_z = -\sqrt{3}cdP_2(\cos\beta)J(\omega_N)$$

$$\eta_{xy} = -\frac{\sqrt{3}}{6}cdP_2(\cos\beta)[4J(0) + 3J(\omega_N)] \quad (2)$$

in which $d = (\mu_0 h\gamma_H\gamma_N)/(8\pi^2 r_{NH}{}^3)$, $c = \gamma_N B_0\Delta\sigma/\sqrt{3}$, μ_0 is the permeability of free space, h is Planck's constant, γ_H and γ_N are the gyromagnetic ratios for ^{1}H and ^{15}N, respectively, r_{NH} is the distance between the two nuclei, B_0 is the static magnetic field strength, $\Delta\sigma = \sigma_\parallel - \sigma_\perp$, the principal components of the ^{15}N CSA tensor are $\sigma_\parallel$ and $\sigma_\perp$, and $P_2(x) = (3x^2 - 1)/2$.

The rate constants for auto relaxation of longitudinal S_z magnetization, transverse S_x (or S_y) magnetization, $2I_zS_z$ longitudinal two spin order, and $2I_zS_x$ (or $2I_zS_y$) transverse antiphase coherence are given by respectively[36]

$$R_1 = (d^2/4)[3J(\omega_N) + J(\omega_H - \omega_N) + 6J(\omega_H + \omega_N)] + c^2J(\omega_N)$$

$$R_2 = (d^2/8)[4J(0) + 3J(\omega_N) + J(\omega_H - \omega_N) + 6J(\omega_H) + 6J(\omega_H + \omega_N)] + (c^2/6)[4J(0) + 3J(\omega_N)] + R_{ex}$$

$$R_{1IS} = (d^2/4)[3J(\omega_N) + 3J(\omega_H)] + c^2J(\omega_N) + R_{1I}$$

$$R_{2IS} = (d^2/8)[4J(0) + 3J(\omega_N) + J(\omega_H - \omega_N) + 6J(\omega_H + \omega_N)] + (c^2/6)[4J(0) + 3J(\omega_N)] + R_{ex} + R_{1I} \quad (3)$$

in which R_{ex} represents the additive effect of chemical exchange line broadening and R_{1I} is the longitudinal relaxation rate constant resulting from dipolar interactions between the amide $^1H^N$ spin and other remote protons that are near in space.

The method proposed by Tjandra et al. for measuring η_{xy}[26] is reviewed briefly in order to provide a basis for the method developed for measuring η_z. A pulse sequence for measuring η_{xy} is shown in Figure 1a; this sequence is a simple modification of existing pulse sequences.[26,40] An initial INEPT[41] period converts equilibrium I_z magnetization into $2I_zS_y$ antiphase coherence. During the relaxation time period τ, cross relaxation occurs between $2I_zS_y$ and S_y coherences. The ^{15}N 180° pulse at $\tau/2$ refocuses evolution under ^{15}N chemical shift and the ^{1}H−^{15}N scalar coupling Hamiltonians; however, scalar coupling evolution during each period $\tau/2$ serves to average the auto relaxation rates of the in-phase and antiphase coherences.[42,43] If $\tau = n/J$, where n is an integer and J is the one-bond N−H scalar coupling constant, then the effective evolution during the relaxation period τ is given by

$$\frac{d}{dt}\begin{bmatrix}\langle S_y\rangle(\tau)\\ \langle 2I_zS_y\rangle(\tau)\end{bmatrix} = -\begin{bmatrix}\bar{R}_2 & \eta_{xy}\\ \eta_{xy} & \bar{R}_2\end{bmatrix}\begin{bmatrix}\langle S_y\rangle(\tau)\\ \langle 2I_zS_y\rangle(\tau)\end{bmatrix} \quad (4)$$

in which $\bar{R}_2 = (R_2 + R_{2IS})/2$. The density operator at the beginning of τ is given by $\sigma(0) = <2I_zS_y>(0)2I_zS_y$. Consequently, the density operator at time τ is given by

$$\sigma(\tau) = [\exp(-\bar{R}_2\tau)\cosh(\eta_{xy}\tau)2I_zS_y + \exp(-\bar{R}_2\tau)\sinh(\eta_{xy}\tau)S_y]\langle 2I_zS_y\rangle(0) \quad (5)$$

The pulse sequence is executed twice for each value of τ. Whether S_y or $2I_zS_y$ coherence present at the end of τ is transferred to detectable ^{1}H coherence is determined by the values of τ_a and τ_b in Figure 1a. The first experiment selects for the in-phase S_y operator, with resulting signal I_{cross}, by setting $\tau_a = \Delta + t_1/2$ and $\tau_b = t_1/2$, in which $\Delta = 1/(4J)$. In addition, a composite 90° ^{1}H pulse is inserted prior to gradient G5 to dephase the antiphase coherence. The second experiment selects for the antiphase $2I_zS_y$ coherence, with resulting signal intensity I_{auto}, by setting $\tau_a = t_1/2$ and $\tau_b = \Delta + t_1/2$ and omitting the composite pulse. The ^{15}N coherences are converted to detectable ^{1}H magnetization using the gradient-selected preservation of equivalent pathways (PEP) scheme.[44,45] The ratio of the two signal intensities has the functional form of a hyperbolic tangent from which η_{xy} can be determined by nonlinear least-squares optimization:[26]

$$I_{cross}/I_{auto} = \langle S_y\rangle(\tau)/\langle 2I_zS_y\rangle(\tau) = \tanh(\eta_{xy}\tau) \quad (6)$$

An experiment designed to measure the longitudinal cross-correlation relaxation rate constant η_z by an analogous method must explicitly average the relaxation rates for the S_z and $2I_zS_z$ operators because these operators commute with the scalar coupling Hamiltonian. In addition, dipolar cross relaxation between I_z and S_z spin operators and ^{1}H−^{15}N dipolar/^{1}H CSA interference between I_z and $2I_zS_z$ spin operators must be suppressed.

(37) Woessner, D. E. *J. Chem. Phys.* **1962**, *37*, 647−654.
(38) Barbato, G.; Ikura, M.; Kay, L. E.; Pastor, R. W.; Bax, A. *Biochemistry* **1992**, *31*, 5269−5278.
(39) Brüschweiler, R. *Chem. Phys. Lett.* **1996**, *257*, 119−122.
(40) Tessari, M.; Vis, H.; Boelens, R.; Kaptein, R.; Vuister, G. W. *J. Am. Chem. Soc.* **1997**, *119*, 8985−8990.
(41) Morris, G. A.; Freeman, R. *J. Am. Chem. Soc.* **1979**, *101*, 760−762.
(42) Vold, R. R.; Vold, R. L. *J. Chem. Phys.* **1976**, *64*, 320−332.
(43) Palmer, A. G.; Skelton, N. J.; Chazin, W. J.; Wright, P. E.; Rance, M. *Mol. Phys.* **1992**, *75*, 699−711.
(44) Palmer, A. G.; Cavanagh, J.; Wright, P. E.; Rance, M. *J. Magn. Reson.* **1991**, *93*, 151−170.
(45) Kay, L. E.; Keifer, P.; Saarinen, T. *J. Am. Chem. Soc.* **1992**, *114*, 10663−10665.

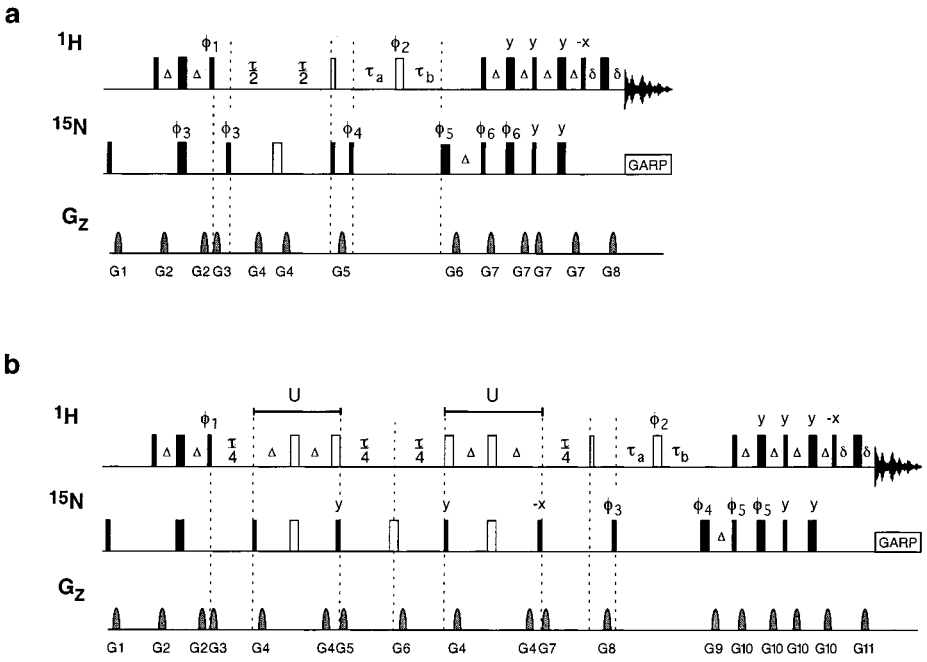

Figure 1. Pulse sequences for measurement of (a) transverse η_{xy} and (b) longitudinal η_z ^{1}H$-^{15}$N dipolar/^{15}N CSA relaxation interference rate constants. Narrow and wide bars correspond to 90 and 180° pulses, respectively. Solid bars represent rectangular pulses, while open bars correspond to composite ($90°_x-90°_y$) 90° and composite ($90°_y-180°_x-90°_y$) 180° pulses. All pulses are applied with phase x unless specified otherwise. Delay durations are $\Delta = 2.67$ ms and $\delta = 0.75$ ms. Two experiments were performed for each value of the relaxation period τ. In the first experiment the composite ^{1}H 90° pulse, designated by the narrow open bar, is included, $\tau_a = \Delta$ and $\tau_b = \Delta + t_1/2$. In the second experiment, the composite 90° pulse is absent, $\tau_a = \Delta + t_1/2$ and $\tau_b = t_1/2$. The phase cycling is the following: (a) $\phi_1 = -y, -y, y, y$; $\phi_2 = 4(x), 4(-x)$; $\phi_3 = 4(x), 4(-x)$; $\phi_4 = 8(x), 8(-x)$; $\phi_5 = x, y, -x, -y$; $\phi_6 = x$; receiver $= x, -x, -x, x, 2(-x, x, x, -x), x, -x, -x, x$. (b) $\phi_1 = -y, -y, y, y$; $\phi_2 = 4(x), 4(-x)$; $\phi_3 = 8(x), 8(-x)$; $\phi_4 = x, y, -x, -y$; $\phi_5 = x$; receiver $= 2(x, -x, -x, x), 2(-x, x, x, -x)$. Gradients along the z-axis have rectangular amplitude profiles, with gradient powers and durations equal to the following: (a) G1 = 5.4 G/cm, 1.0 ms; G2 = 4.0 G/cm, 0.5 ms; G3 = 8.0 G/cm, 0.5 ms; G4 = 6.0 G/cm, 0.5 ms; G5 = 8.6 G/cm, 0.5 ms; G6 = −32.4 G/cm, 1.25 ms; G7 = 5.5 G/cm, 0.5 ms; G8 = 32.4 G/cm, 0.125 ms. (b) G1 = 5.4 G/cm, 1.0 ms; G2 = 4.0 G/cm, 0.5 ms; G3 = 9.5 G/cm, 0.5 ms; G4 = 6.0 G/cm, 0.5 ms; G5 = 9.0 G/cm, 0.5 ms; G6 = 8.6 G/cm, 0.5 ms; G7 = 10.0 G/cm, 0.5 ms; G8 = 9.5 G/cm, 0.5 ms; G9 = −32.4 G/cm, 1.25 ms; G10 = 6.0 G/cm, 0.5 ms; G11 = 32.4 G/cm, 0.125 ms. Gradient PEP coherence selection is obtained by inverting the sign of gradient G6 and phase ϕ_6 in (a) and gradient G9 and phase ϕ_5 in (b).[45]

The coupled evolution of longitudinal magnetization and two spin order is described by[35,46]

$$\mathbf{M}_z(\tau) = \exp(-\mathbf{R}\tau)\mathbf{M}_z(0) \tag{7}$$

$$\mathbf{M}_z(t) = \begin{bmatrix} \langle S_z\rangle(t) \\ \langle 2I_zS_z\rangle(t) \end{bmatrix} \tag{8}$$

$$\mathbf{R} = \begin{bmatrix} R_1 & \eta_z \\ \eta_z & R_{1IS} \end{bmatrix} \tag{9}$$

In the writing of eqs 7−9, the assumptions have been made that contributions to the evolution from the ^{1}H and ^{15}N steady-state magnetizations have been removed by subtracting pairs of experiments in which the sign of $\mathbf{M}_z(0)$ is alternated,[47] that small effects of ^{1}H$-^{15}$N dipolar cross relaxation and ^{1}H$-^{15}$N dipole/^{1}H CSA relaxation interference have been suppressed by inverting all S_z operators at time $\tau/2$,[46] and that dipolar interactions between the ^{1}H^N spin and remote protons have been minimized by high-level replacement of nonexchangeable protons by deuterons.

In the experimental protocol considered, the density operator at the beginning of the relaxation period τ is given by $\sigma(0) = <2I_zS_z>(0)2I_zS_z$. As for the transverse cross-correlation experiment, two spectra are recorded in which I_{cross} represents the intensity of signal resulting from the transfer from $2I_zS_z$ to S_z during τ, and I_{auto} represents the intensity of signal resulting from relaxation of $2I_zS_z$ during τ. If no additional averaging of the relaxation rate matrix is performed, then

$$I_{cross}/I_{auto} = [\exp(-\mathbf{R}\tau)]_{12}/[\exp(-\mathbf{R}\tau)]_{22} \tag{10}$$

in which $[\exp(-\mathbf{R}\tau)]_{ij}$ is the i,jth element of the matrix exponential, obtained from eqs 7−9. If the auto relaxation rate constants R_1 and R_{1IS} are averaged identically to $\bar{R}_1 = (R_1 + R_{1IS})/2$, then the relaxation matrix takes the form

$$\bar{\mathbf{R}} = \begin{bmatrix} \bar{R}_1 & \eta_z \\ \eta_z & \bar{R}_1 \end{bmatrix} \tag{11}$$

and the ideal result obtained is, in complete analogy to eqs 4−6,

$$\sigma(\tau) = [\exp(-\bar{R}_1\tau)\cosh(\eta_z\tau)2I_zS_z + \exp(-\bar{R}_1\tau)\sinh(\eta_z\tau)S_z]\langle 2I_zS_z\rangle(0) \tag{12}$$

and

$$I_{cross}/I_{auto} = \langle S_z\rangle(\tau)/\langle 2I_zS_z\rangle(\tau) = \tanh(\eta_z\tau) \tag{13}$$

The ratios I_{cross}/I_{auto} for eqs 10 and 13 are plotted versus τ in Figure 2a, assuming typical values of relaxation rates for ^{2}H/^{15}N-labeled *E. coli* RNaseH. As can be seen the functional

(46) Boyd, J.; Hommel, U.; Campbell, I. D. *Chem. Phys. Lett.* **1990**, *175*, 477−482.

(47) Sklenar, V.; Torchia, D.; Bax, A. *J. Magn. Reson.* **1987**, *73*, 375−379.

dependence arising from the unaveraged rate matrix diverges drastically from the desired hyperbolic tangent. The relaxation matrix can be averaged to first order in τ by applying a transformation, **U**, at $\tau/2$ that exchanges the magnitudes of the S_z and $2I_zS_z$ operators. If the transformation is represented by

$$\mathbf{U} = \begin{bmatrix} 0 & 1 \\ 1 & 0 \end{bmatrix} \tag{14}$$

then the density operator at the end of the relaxation period is given by

$$\begin{aligned} \mathbf{M}_z(\tau) &= \exp(-\mathbf{R}\tau/2)\mathbf{U}\exp(-\mathbf{R}\tau/2)\mathbf{M}_z(0) \\ &= \mathbf{U}\exp(-\mathbf{URU}\tau/2)\exp(-\mathbf{R}\tau/2)\mathbf{M}_z(0) \\ &\approx \mathbf{U}\{\mathbf{E} - \bar{\mathbf{R}}\tau + ...\}\mathbf{M}_z(0) \end{aligned} \tag{15}$$

The ratio I_{cross}/I_{auto} obtained from eq 15 is plotted versus τ in Figure 2a. As expected, good agreement is obtained over the linear portion of the hyperbolic tangent function. The relaxation matrix can be averaged to second order in time by applying the transformations **U** at times $\tau/4$ and $3\tau/4$ to give a density operator

$$\begin{aligned} \mathbf{M}_z(\tau) &= \exp(-\mathbf{R}\tau/4)\mathbf{U}\exp(-\mathbf{R}\tau/2)\mathbf{U}\exp(-\mathbf{R}\tau/4)\mathbf{M}_z(0) \\ &= \mathbf{U}\exp(-\mathbf{URU}\tau/4)\exp(-\mathbf{R}\tau/2)\times \\ &\qquad \exp(-\mathbf{URU}\tau/4)\mathbf{UM}_z(0) \\ &\approx \mathbf{U}\{\mathbf{E} - \bar{\mathbf{R}}\tau + \bar{\mathbf{R}}^2\tau^2/2 + ...\}\mathbf{UM}_z(0) \\ &\approx \{\mathbf{E} - \bar{\mathbf{R}}\tau + \bar{\mathbf{R}}^2\tau^2/2 + ...\}\mathbf{M}_z(0) \end{aligned} \tag{16}$$

at the end of the relaxation period τ. The ratio I_{cross}/I_{auto} obtained from eq 16 is plotted versus τ in Figure 2a. The results show that the second-order averaging of the relaxation matrix provides nearly ideal results for times up to $\tau \approx 1.5/\bar{R}_1 = 3/(R_1 + R_{1IS})$. Higher order averaging of the relaxation rate matrix is possible but unnecessary in the present application in which high-level deuteration has been used to minimize dipolar interactions between amide $^1H^N$ spins and remote protons. In protonated molecules, $R_{1IS} \gg R_1$ because $R_{1I} \gg R_1$; as a result, the maximum value of τ for which the averaging procedure is effective is reduced. Figure 2b illustrates the maximum value of $I_{cross}/I_{auto} = \tanh[3\eta_z/(R_1 + R_{1IS})]$ for which the relaxation matrix is averaged effectively as a function of rotational correlation time for $^2H/^{15}N$-labeled proteins.

A pulse sequence that incorporates the second-order averaging procedure is given in Figure 1b. Beginning with equilibrium proton magnetization, an INEPT period generates $2I_zS_z$ two-spin order prior to the first $\tau/4$ period. Inversion of the phase of ϕ_1 serves to remove contributions from the steady-state magnetizations.[47] Gradient G3 dephases other coherences. The 180° ^{15}N composite pulse in the middle of the relaxation period τ serves to suppress $^1H-^{15}N$ dipolar cross relaxation and $^1H-^{15}N$ dipolar/^1H CSA interference.[46] The sequence elements labeled *U* incorporate the transformation represented by the matrix **U**; similar pulse sequence elements have been used for spin-state selective coherence transfer.[48] As long as $(2\pi J)^2 \gg (R_{1IS} - R_1)^2$, a condition well satisfied in the present application, in which $2\pi J = 580\ s^{-1}$ and $R_{1IS} - R_1 \approx R_{1I} \leq 20\ s^{-1}$, the

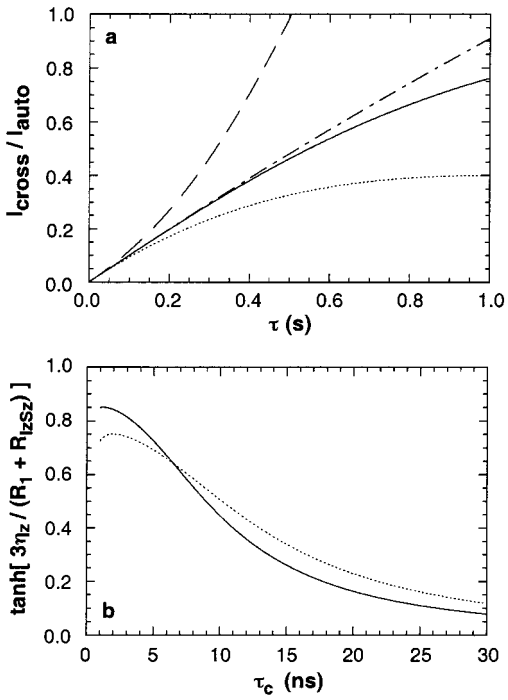

Figure 2. Theoretical results for the ratio I_{cross}/I_{auto}. In (a), theoretical curves for I_{cross}/I_{auto} resulting from increasing orders of averaging of the rate matrix given by eqs (− −) 10, (···) 15, and (− - −) 16 are compared to the ideal behavior given by (—) eq 13 for highly deuterated RNaseH. In (b) the maximum signal amplitude $I_{cross}/I_{auto} = \tanh(3\eta_z/(R_1 + R_{1IS}))$ is plotted as a function of rotational correlation time for Larmor frequencies of (···) 500 MHz and (—) 800 MHz. Values typical for $^2H/^{15}N$ *E. coli* RNaseH were used: $R_1 = 1.6\ s^{-1}$, $\eta_z = 1.0\ s^{-1}$, and $R_{1IS} = 4.6\ s^{-1}$ was approximated to be the sum of nitrogen and proton longitudinal relaxation with $R_{1I} = 3\ s^{-1}$. As described in the text, inversion of the ^{15}N spins at $\tau/2$ is necessary to suppress effects of $^1H-^{15}N$ dipolar cross relaxation and $^1H-^{15}N$ dipole/^1H CSA interference. Numerical calculations including these additional effects yield curves indistinguishable from those plotted. Numerical calculations were performed using Mathematica (Wolfram Research).

matrix **U** is given by[49]

$$\mathbf{U} = -\sin(2\pi J\Delta)\exp(-2\bar{R}_2\Delta)\begin{bmatrix} 0 & 1 \\ 1 & 0 \end{bmatrix} \tag{17}$$

The factors $-\sin(2\pi J\Delta)\exp(-2\bar{R}_2\Delta)$ affect both the S_z and $2I_zS_z$ operators equally; consequently, variations in the scalar coupling constants *J* and relaxation rates for different spins affect the overall sensitivity of the experiment but do not affect the time dependence of I_{cross}/I_{auto}. Gradients G5 and G7, immediately following the sequence elements *U*, dephase coherences resulting from mistuning of the delay Δ. Pulse phases have been arranged so that the sign of the *S* spin operators are inverted relative to *I* spin operators during *U* to further improve suppression of $^1H-^{15}N$ dipolar cross relaxation and $^1H-^{15}N$ dipolar/^1H CSA interference. Frequency-labeling and transfer of ^{15}N coherence to ^1H coherence for acquisition is identical to Figure 1a.

Both pulse sequences in Figure 1 use gradient G3 to dephase the solvent magnetization. In principle, saturation of the solvent resonance can be avoided by applying selective 90° water flip back pulses[50] to the solvent signal prior to gradients G3 and

(48) Sørensen, M. D.; Meissner, A.; Sørensen, O. W. *J. Biomol. NMR* **1997**, *10*, 181−186.

(49) Cavanagh, J.; Fairbrother, W. J.; Palmer, A. G.; Skelton, N. J. *Protein NMR Spectroscopy: Principles and practice*; Academic Press: San Diego, CA, 1996.

(50) Grzesiek, S.; Bax, A. *J. Am. Chem. Soc.* **1993**, *115*, 12593−12594.

G5 in Figure 1a and gradients G3 and G8 in Figure 1b. However, in the present application, the potential errors arising from the off-resonance effects of these pulses may constitute a greater disadvantage than the sensitivity losses associated with saturating solvent magnetization.

Experimental Section

Sample Preparation. *Escherichia coli* strain BL21(DE3) (Novagen) transformed with the expression plasmid used in previous studies[34] was used to produce $^2H/^{15}N$ isotopically enriched RNaseH. To allow the bacteria to acclimate to deuterated growth media, cells were first grown to log phase in M9 minimal medium[51] containing 34% D_2O and natural abundance NH_4Cl. An aliquot of these cells were used as an inoculum for growth in 68% D_2O, 100% $^{15}NH_4Cl$ M9 minimal medium. When this culture reached log phase, an aliquot was used to inoculate 4 L of M9 minimal medium containing 99.8% D_2O and 100% $^{15}NH_4Cl$. Glucose was provided at natural isotopic abundance. Expression of RNaseH was induced by the addition of isopropyl β-D-thiogalactopyranoside (IPTG) to a final concentration of 1 mM when the culture optical density at 600 nm reached 0.8. Cells were harvested 6−12 h after induction by centrifugation and lysed by sonication in 20 mM NaCl, 50 mM *N*-(2-hydroxyethyl)piperazine-*N*′-2-ethanesulfonic acid (HEPES), 10 mM $MgCl_2$, 0.5 mM ethylenediaminetetraacetic acid (EDTA), and 1 mM β-mercaptoethanol. The cell lysate was passed over macro Q ion exchange and heparin affinity chromatography columns (Biorad). *E. coli* RNaseH does not bind to the macro Q anion exchanger but binds the heparin resin at low ionic strength.[52] RNaseH was eluted from the heparin column using a buffer containing 400 mM NaCl, 50 mM HEPES, 10 mM $MgCl_2$, 0.5 mM EDTA, and 1 mM β-mercaptoethanol. Further purification was performed as described elsewhere.[34] The efficiency of replacement of nonexchangeable protons with deuterons was estimated using laser desorption mass spectrometry (University of Michigan Protein and Carbohydrate Structure Facility). The measured mass of the $^2H/^{15}N$-labeled RNaseH was 18 727 Da. A control sample of RNaseH containing natural abundance isotopes yielded a measured mass of 17 608 Da (compared with a value of 17 597 Da predicted from the protein sequence). RNaseH contains 919 nonexchangeable proton sites and 227 nitrogen sites. The difference between the measured masses of the isotopically enriched and natural abundance samples indicates that, on average, 892 or approximately 97% of the nonexchangeable protons are replaced with deuterons.

NMR Spectroscopy. All experiments were performed on a Varian Inova 500 NMR spectrometer operating at a ^1H Larmor frequency of 499.88 MHz and a ^{15}N Larmor frequency of 50.66 MHz. All measurements were made on a single 0.8 mM $^2H/^{15}N$-enriched RNaseH sample (100 mM $NaCO_2CD_3$, 1 mM dithiothreitol-d_{10}, 2 mM NaN_3, 90%/10% H_2O/D_2O, pH 5.5). The sample temperature was calibrated to 300 K using a methanol standard and regulated with the Varian VT unit. All experiments performed used spectral widths of 2.18 kHz × 12.5 kHz in the $t_1 \times t_2$ dimensions, except for the R_2 experiment, which used a spectral width of 2.72 kHz in the t_1 dimension. The ^1H carrier was set to the frequency of the water resonance (4.73 ppm), and the ^{15}N carrier frequency was set to 116 ppm. Decoupling of ^{15}N spins during acquisition was performed using the GARP-1 composite pulse sequence[53] with a radio frequency field strength of 1.0 kHz. Hypercomplex quadrature detection using the PEP sensitivity-enhanced gradient method was employed during t_1 evolution periods.[45,54]

Auto Relaxation Measurements and NOE. R_1, R_2, and the $\{^1H\}^{15}N$ steady-state heteronuclear NOE for the ^{15}N nuclei in RNaseH were measured by two-dimensional sensitivity-enhanced proton-detected heteronuclear NMR spectroscopy using inversion recovery, Carr−Purcell−Meiboom−Gill (CPMG), and steady-state NOE pulse sequences described previously.[55−57] For all experiments, 180 × 3072 complex points were acquired in the $t_1 \times t_2$ dimensions. Proton decoupling during the relaxation period of R_1 measurements was performed using a train of cosine modulated 180° pulses at 5 ms intervals.[46,57] The number of replicates of each time point and the experimental time points for R_1 measurements were 3 × 0.000 s, 2 × 0.060 s, 2 × 0.130 s, 1 × 0.200 s, 1 × 0.290 s, 2 × 0.600 s, 2 × 0.850 s, 1 × 1.250 s, and 2 × 1.420 s. The R_2 measurements were performed with a delay $\tau_{cp} = 1.0$ ms between the centers of the 85 μs ^{15}N 180° pulses in the CPMG pulse train; proton decoupling was obtained by applying 180° pulses synchronously with even spin−echoes during the CPMG pulse train.[43,58] Time points for R_2 measurements were 3 × 0.000 s, 2 × 0.016 s, 2 × 0.032 s, 3 × 0.048 s, 1 × 0.064 s, 1 × 0.080 s, 2 × 0.112 s, 2 × 0.160 s, and 1 × 0.288 s. R_1 and R_2 experiments used a recycle delay of 2.5 s between transients and 8 transients per t_1 increment. The NOE was measured from pairs of spectra recorded with (NOE) and without (CONTROL) proton saturation during the recycle delay. The NOE and CONTROL pairs were acquired with each t_1 point interleaved. Proton saturation during the NOE experiments was obtained by applying a train of nonselective 120° ^1H pulses every 5 ms for 4 s. A 12 s delay preceded the first transient for each CONTROL t_1 point to permit ^1H magnetization to reach equilibrium. Subsequent CONTROL transients used a 5 s recycle delay. The NOE and CONTROL measurements were performed using a total of 16 transients per t_1 increment. Both experiments were performed four times. The total acquisition times for R_1, R_2, and NOE measurements were approximately 44, 40, and 62 h, respectively.

Dipolar-CSA Relaxation Interference. NMR experiments for measuring longitudinal and transverse $^1H-^{15}N$ dipolar/^{15}N CSA cross-correlation rate constants were performed using the pulse schemes depicted in Figure 1. For both cross relaxation experiments, either 32 or 48 transients were averaged per t_1 increment in the experiments used to measure I_{cross}, and 16 transients were averaged per t_1 increment in the experiments used to measure I_{auto}; 180 × 4096 complex data points were acquired in the $t_1 \times t_2$ dimensions. Relaxation delays used for the η_z measurement were 0.150, 0.225, 0.300, 0.375, and 0.450 s. Relaxation delays for the η_{xy} measurement were 0.0320, 0.0534, 0.0748, 0.0961, and 0.1068 s. The remaining experimental parameters were identical to the auto relaxation experiments. The total acquisition times for the η_z and η_{xy} cross-correlation measurements were approximately 95 and 90 h, respectively.

Data Processing. NMR data were processed using Felix 2.30 (MSI) and in-house FORTRAN programs on SGI Indigo workstations. A 6 Hz exponential apodization function applied to the free induction decays and a Kaiser apodization function with $\phi = \pi$ was applied to the t_1 interferograms.[59] Data were zero filled to 8192 points prior to Fourier transformation, and a second-order polynomial baseline correction was applied in the acquisition dimension after Fourier transformation. Peak heights were measured from the NMR spectra using routines written in the Felix macro language. For the determination of auto relaxation rates, peak heights and uncertainties were determined from duplicate spectra as described previously.[56,60] R_1 and R_2 values were determined by nonlinear least-squares fitting of the experimental data to two parameter monoexponential equations.[60] The value of σ_{NH} was determined as

$$\sigma_{NH} = (\gamma_N/\gamma_H)R_1(\mathrm{NOE} - 1) \qquad (18)$$

in which NOE is the ratio of signal intensities in the NOE and

(51) Sambrook, J.; Fritsch, E. F.; Maniatis, T. *Molecular Cloning: A Laboratory Manual*; Cold Spring Harbor Laboratory: Cold Spring Harbor, NY, 1982.
(52) Dabora, J. M.; Marqusee, S. *Prot. Sci.* **1994**, *3*, 1401−1408.
(53) Shaka, A. J.; Barker, P. B.; Freeman, R. *J. Magn. Reson.* **1985**, *64*, 547−552.
(54) Marion, D.; Ikura, M.; Tschudin, R.; Bax, A. *J. Magn. Reson.* **1989**, *85*, 393−399.
(55) Kördel, J.; Skelton, N. J.; Akke, M.; Palmer, A. G.; Chazin, W. J. *Biochemistry* **1992**, *31*, 4856−4866.
(56) Skelton, N. J.; Palmer, A. G.; Akke, M.; Kördel, J.; Rance, M.; Chazin, W. J. *J. Magn. Reson., Ser. B* **1993**, *102*, 253−264.
(57) Farrow, N. A.; Muhandiram, R.; Singer, A. U.; Pascal, S. M.; Kay, C. M.; Gish, G.; Shoelson, S. E.; Pawson, T.; Forman-Kay, J. D.; Kay, L. E. *Biochemistry* **1994**, *33*, 5984−6003.
(58) Kay, L. E.; Nicholson, L. K.; Delagio, F.; Bax, A.; Torchia, D. A. *J. Magn. Reson.* **1992**, *97*, 359−375.
(59) Ernst, R. R.; Bodenhausen, G.; Wokaun, A. *Principles of nuclear magnetic resonance in one and two dimensions*; Clarendon Press: Oxford, U.K., 1987.

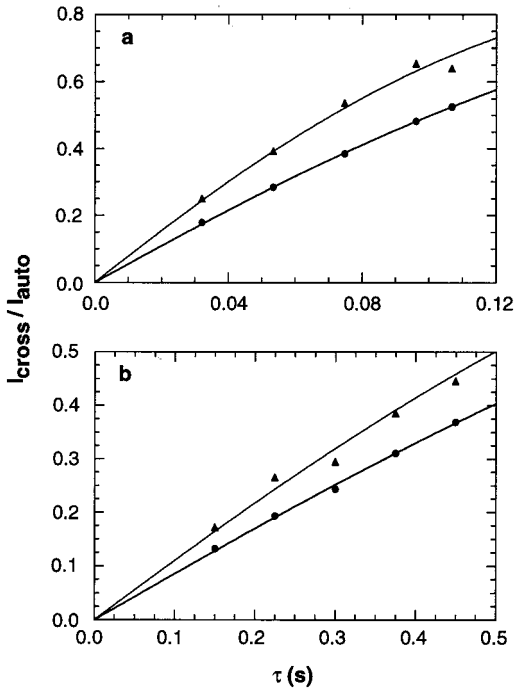

Figure 3. Experimental measurements of I_{cross}/I_{auto} for (a) transverse and (b) longitudinal cross-correlation experiments for residues (●) E61 and (▲) W90 in RNaseH. The solid lines drawn are fits of the data to (a) eq 6 and (b) eq 13.

CONTROL experiments. For the cross relaxation experiments, cross-peak intensity ratios I_{cross}/I_{auto} were determined after normalization for number of transients recorded in each experimental scheme. The ratios were fit to eqs 13 and 6 using an in-house FORTRAN program. Uncertainties in η_z and η_{xy} values were obtained using the jackknife procedure.[61]

Results

Relaxation Rate Constants. The longitudinal, η_z, and transverse, η_{xy}, cross-correlation rate constants reflecting ^{1}H−^{15}N dipolar/^{15}N CSA interference were measured in ^{2}H/^{15}N-enriched RNaseH using the pulse sequences shown in Figure 1. Representative plots of I_{cross}/I_{auto} for the longitudinal and transverse cross correlation experiments are shown in Figure 3. In both experiments, extracting the relaxation rate constants from I_{cross}/I_{auto} requires that the diagonal elements of the relaxation matrix be identical. In the experiment used to measure transverse cross-correlation,[26] averaging of the relaxation rates R_2 and R_{2IS} during the delay τ occurs as a consequence of scalar coupling between the ^{15}N and ^{1}H nuclei. In the new experiment used to measure η_z, averaging of R_1 and R_{1IS} occurs during a pair of pulse-interrupted free-precession periods. Numerical simulations shown in Figure 2 indicate the accuracy of the averaging procedure for time periods up to ∼1.5/$\bar{R}_1 = 3/(R_1 + R_{1IS})$. The value of R_{1I} for the amide ^{1}H spins in ^{2}H/^{15}N RNaseH was estimated to be ∼3 s^{-1} from measurements of the relaxation of $2I_zS_z$ coherence (data not shown). Using this estimate together with $R_1 = 1.6$ s^{-1} yields $\bar{R}_1 \approx 3.1$ s^{-1}. Data were well fit by eq 13 for time points up to 0.45 s, which agrees well with the theoretical predictions; deviations from the theoretical curve were observed for longer times (not shown). The cross-correlation rate constants were quantified for 91 well-resolved RNaseH backbone amide resonances in ^{2}H/^{15}N-labeled RNaseH. The rate constants are given in Supporting Information. For 61 ^{15}N spins located in secondary structural elements, η_z values range from 0.845 to 1.13 s^{-1} with a median of 1.01 s^{-1}, and η_{xy} ranges from 5.53 to 8.83 s^{-1} with a median of 7.62 s^{-1}. The R_1, R_2, and σ_{NH} rate constants were measured for the same 91 residues and are given in the Supporting Information. For ^{15}N spins in secondary structure elements, the ranges for R_1, R_2, and σ_{NH} values are 1.37−1.68 s^{-1}, 9.62−12.7 s^{-1}, and 0.0241−0.0656 s^{-1}, with respective medians of 1.56 s^{-1}, 11.4 s^{-1}, and 0.0334 s^{-1}.

The theoretical expression for the η_{xy}/η_z ratio obtained from eq 2 is

$$\frac{\eta_{xy}}{\eta_z} = \frac{4J(0) + 3J(\omega_N)}{6J(\omega_N)} \tag{19}$$

The quantitative accuracy of the η_{xy}/η_z ratios was verified by comparison with the auto relaxation rate constants. The theoretical expressions for the rates given in eqs 2 and 3 indicate that R_2/R_1 and η_{xy}/η_z differ only in high-frequency terms of the spectral density function (i.e. terms $J(\omega)$ where ω is of the order $\omega_H \pm \omega_N$). The high-frequency spectral density values can be approximated from the heteronuclear cross relaxation rate, σ_{NH}, using the reduced spectral density mapping approach,[4] which approximates R_1, R_2, and σ_{NH} as

$$R_1 = (d^2/4)[3J(\omega_N) + 7J(0.921\omega_H)] + c^2J(\omega_N)$$

$$R_2 = (d^2/8)[4J(0) + 3J(\omega_N) + 13J(0.955\omega_H)] + (c^2/6)[4J(0) + 3J(\omega_N)] + R_{ex}$$

$$\sigma_{NH} = (5d^2/4)J(0.870\omega_H) \tag{20}$$

Assuming that the high-frequency spectral density terms are given by $J(\epsilon\omega_H) = (0.870/\epsilon)^2J(0.870\omega_H)$, the relationship between the autorelaxation and cross-correlation rate constant can be written as

$$\frac{R_2 - 1.079\sigma_{NH}}{R_1 - 1.249\sigma_{NH}} = \frac{4J(0) + 3J(\omega_N)}{6J(\omega_N)} + \frac{R_{ex}}{R_1 - 1.249\sigma_{NH}} = \frac{\eta_{xy}}{\eta_z} + \frac{R_{ex}}{R_1 - 1.249\sigma_{NH}} \tag{21}$$

For most backbone ^{15}N nuclei in RNaseH, $J(0)$ and $J(\omega_N)$ are at least 1 order of magnitude larger than $0.870J(\omega_H)$.[34] Therefore, the contribution of the high-frequency spectral density terms to the rates R_1 and R_2 are small. Averaging over the 91 quantified resonances, $1.249\sigma_{NH}$ is 2.5% of R_1, and $1.079\sigma_{NH}$ is 0.4% of R_2. The weighted mean η_{xy}/η_z and $(R_2 - 1.079\sigma_{NH})/(R_1 - 1.249\sigma_{NH})$ ratios for 61 ^{15}N spins located in secondary structure elements are 7.53 ± 0.14 and 7.35 ± 0.12, respectively.

The ratio η_{xy}/η_z versus $(R_2 - 1.079\sigma_{NH})/(R_1 - 1.249\sigma_{NH})$ is plotted in Figure 4. As predicted by eq 21, in the absence of chemical exchange contributions to R_2, the data points lie near a line of slope unity. The correlation coefficient between the two quantities is 0.92; the weighted mean root square deviation of the 91 data points from the line of slope unity is 0.27. Data points that are located to the right of the line have increased R_2 values due to a chemical exchange term, R_{ex}, as is the case for the most extreme outlier in the plot, W90 (vide infra). Excluding W90, the remaining 90 data points were fit to a line of slope 1.036 ± 0.046 and y-intercept −0.12 ± 0.32 using formulas appropriate for linear least-squares fitting of data with uncertain-

(60) Palmer, A. G.; Rance, M.; Wright, P. E. *J. Am. Chem. Soc.* **1991**, *113*, 4371−4380.

(61) Mosteller, F.; Tukey, J. W. *Data Analysis and Regression. A Second Course in Statistics*; Addison-Wesley: Reading, MA, 1977.

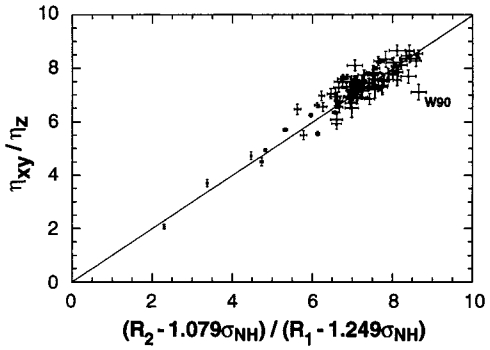

Figure 4. Comparisons of η_{xy}/η_z and $(R_2 - 1.079\sigma_{NH})/(R_1 - 1.249\sigma_{NH})$ ratios for RNaseH. To permit quantitative comparisons, the high-frequency terms in the expressions for R_1 and R_2 in eq 3 are removed by reduced spectral density mapping using eq 21 as described in the text.

ties in both dimensions.[62] Uncertainties in the fitting parameters were determined using the jackknife procedure.[61] Data points with very low R_2/R_1 ratios, generally the C-terminal residues in RNaseH, have larger contributions from high-frequency spectral density terms, and the approximations inherent to reduced spectral density mapping may not be valid. Therefore, data for these resonances are not necessarily expected to lie on the diagonal, although, in the present case, good agreement is obtained even for the most flexible residues. Two residues located in the secondary structure, W118 and A140, gave η_{xy}/η_z ratios of 6.08 ± 0.21 and 5.92 ± 0.20, which are much lower than the average. These low ratios are obtained because both residues have η_{xy} rate constants $< 6\ s^{-1}$, values typical of ^{15}N spins located within flexible loops in RNaseH. The data for these two residues have not been included in the analyses described below. The reason for this discrepancy is not known and is the subject of additional investigation.

Because the ratio η_{xy}/η_z is independent of chemical exchange effects, variations in this ratio for different ^{15}N spins must arise from differences in the degree of internal motion or differences in the orientations of the N−H bond vectors with respect to the principal axis of an anisotropic rotational diffusion tensor. If the degree of local motion is limited, terms proportional to S^2 are much larger than terms proportional to $(1 - S^2)$ in eq 1, and the η_{xy}/η_z ratio is a function only of the spectral density function for a rigid rotor with an asymmetric rotational diffusion tensor. The diffusion tensor can be calculated from the η_{xy}/η_z ratios using direct nonlinear least-squares optimization[15] or the local diffusion approach[18,20] previously used for estimation of rotational diffusion tensors from R_2/R_1 ratios. The local diffusion approximation was adopted in the present analysis. Local diffusion constants (D_i) are calculated from η_{xy}/η_z ratios by the relation

$$D_i = \frac{1}{6\tau_c} = \frac{\omega_N}{3}\left(6\frac{\eta_{xy}}{\eta_z} - 7\right)^{-1/2} \tag{22}$$

in which τ_c is the correlation time defined by the isotropic rigid rotor spectral density function

$$J(\omega) = \frac{2}{5}\frac{\tau_c}{1 + \omega^2\tau_c^2} \tag{23}$$

(62) Press: W. H.; Flannery, B. P.; Teukolsky, S. A.; Vetterling, W. T. *Numerical Recipes. The Art of Scientific Computing*, 2nd. ed.; Cambridge University Press: Cambridge, U.K., 1986.

Table 1. Rotational Diffusion Tensor for RNaseH[a]

structure[b]	$D_{iso}/10^7$ (s^{-1})[c]	$D_{\|}/D_{\perp}$	θ_{PA} (rad)[d]	ϕ_{PA} (rad)[d]	χ^2 [e]	F[f]
1rnh	1.71 ± 0.01	1.22 ± 0.04	1.39 ± 0.10	6.03 ± 0.07	4.93	35.9
2rn2	1.71 ± 0.01	1.19 ± 0.03	1.28 ± 0.08	6.11 ± 0.08	4.49	41.5
minimized	1.71 ± 0.01	1.17 ± 0.03	1.43 ± 0.09	5.85 ± 0.11	5.70	28.1

[a] Local diffusion constants were determined from η_{xy}/η_z ratios for 70 ^{15}N spins using eq 22 and analyzed to determine the rotational diffusion tensor using eq 24. [b] Structure coordinates were obtained from the Protein Data Bank entries 1rnh and 2rn2. Protons were built onto the structure using Insight (MSI). The protocol used to obtain an energy minimized structure starting from the 1rnh coordinates is described in the text. [c] $D_{iso} = (D_{\|} + 2D_{\perp})/3$. [d] θ_{PA} and ϕ_{PA} are obtained from the transformation matrix **A**. They define the rotation necessary to transform the principal axis of the diffusion tensor in the molecular coordinate frames of the PDB files to the z axis. [e] The reduced χ^2 is normalized by the 66 degrees of freedom in the analysis. [f] The F-statistic compares isotropic and axially symmetric models for the rotational diffusion tensor. The p-values for the probability distribution $F_{3,66}$ are less than 10^{-10} for all three structural models.

The diffusion tensor is calculated from a least-squares solution of the equation

$$D_i = e_i^T\mathbf{A}^T\mathbf{Q}\mathbf{A}e_i \tag{24}$$

in which e_i is the vector of direction cosines for the ith N−H bond vector in a molecular reference frame, **A** is the transformation matrix that relates the molecular frame to the principal axis frame of the diffusion tensor, **Q** is a diagonal matrix with elements $Q_{xx} = (D_{yy} + D_{zz})/2$, $Q_{yy} = (D_{xx} + D_{zz})/2$, and $Q_{zz} = (D_{xx} + D_{yy})/2$, and D_{xx}, D_{yy}, and D_{zz} are the principal values of the diffusion tensor.

Nineteen of the residues analyzed in RNaseH exhibited extensive internal backbone motion, as evidenced in 16 cases by a heteronuclear NOE < 0.65 and in 3 cases by significant motion on time scales greater than 100 ps.[34] For the remaining 70 cross-peaks, atomic coordinates from an *E. coli* RNaseH crystal structure (Protein Data Bank entry 1rnh)[63] were used to fit the local diffusion constants to isotropic ($D_{xx} = D_{yy} = D_{zz} = D$), axially symmetric ($D_{xx} = D_{yy} = D_{\perp}$, $D_{zz} = D_{\|}$), and anisotropic ($D_{xx} \neq D_{yy} \neq D_{zz}$) molecular rotational diffusion tensors by solving eq 24 as previously described.[20] The three models were compared using F-statistical testing.[15,20] The axially symmetric model gives a highly significant improvement compared with the isotropic model ($F = 35.9$, $p < 10^{-10}$), whereas the anisotropic model does not significantly improve upon the axially symmetric model ($F = 0.30$, $p = 0.75$). The results for the axially symmetric tensor are given in Table 1. For an axially symmetric diffusion tensor,[20]

$$D_i = D_{iso} - (D_{\|} - D_{\perp})P_2(\cos\theta_i)/3 \tag{25}$$

where $D_{iso} = (D_{\|} + 2D_{\perp})/3$ and θ_i is the angle between the N−H bond vector and the principal axis frame of the diffusion tensor. Figure 5 shows the set of D_i fit to eq 25 using θ_i obtained from the fitted rotational diffusion tensor. Two residues, E6 and G21, with very precise D_i values give very high residuals, and these are shown in open symbols in Figure 5. The local diffusion constant for E6 is 9.4 standard deviations larger than predicted, and the local diffusion constant for G21 is 5.1 standard deviations smaller than predicted from the measured diffusion tensor. Elimination of the residual errors for E6 and G21 would require physically unrealistic changes

(63) Yang, W.; Hendrickson, W. A.; Crouch, R. J.; Satow, Y. *Science* **1990**, *249*, 1398−1405.

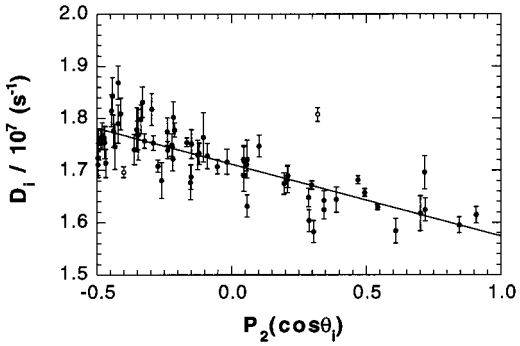

Figure 5. Rotational diffusion tensor. Local diffusion constants D_i determined from η_{xy}/η_z ratios using eq 22 are shown as a function of the orientation of the N−H bond vector in the principal axis frame of the diffusion tensor for RNaseH obtained using the 1rnh structural coordinates. The solid line indicates the fit of the data to eq 25 for the axially symmetric rotational diffusion model. The open circles indicate the data for the two largest outliers, E6 and G21.

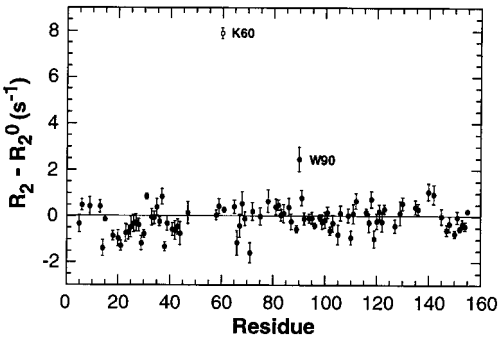

Figure 6. Chemical exchange. Differences between R_2 and R_2^0 are plotted versus residue number for RNaseH. R_2 was measured from a CPMG experiment and R_2^0 was determined from the measured η_{xy}/η_z ratio using eq 26. The exchange value for K60 (open circle) was determined from the η_{xy}/η_z ratio calculated from the rotational diffusion tensor, as described in the text. Residues showing significant chemical exchange >1 s^{-1} are labeled on the graph.

of $>45°$ in the angles between the NH bond vectors and the unique axis of the rotational diffusion tensor.

The calculations of the diffusion tensor from the experimental data were repeated using atomic coordinates obtained from a second crystal structure of RNaseH (Protein Data Bank entry 2rn2)[64] and from an energy-minimized hydrated RNaseH structure. The minimization was performed using Discover (MSI). The protein, represented by the 1rnh structural coordinates, was placed in a box of water molecules, and the energy was minimized using periodic boundary conditions and the cvff force field. Initially, minimization was performed while constraining the protein coordinates to relieve unfavorable contacts with solvent; subsequently, minimization was performed for all coordinates. As shown in Table 1, similar diffusion tensors were obtained for all analyses. The data points corresponding to residues E6 and G21 exhibit the largest deviations from the predicted local diffusion constants for all calculations, which suggests that the large residuals for these two residues are due to a systematic error that affects the cross-relaxation rate measurements, rather than structural considerations such as crystal packing effects. Exclusion of these two outliers from the analysis does not significantly affect the final diffusion tensor, but increases the F statistic comparing the isotropic and axially symmetric diffusion models for the 1rnh structural coordinates to 72.6.

Significant contributions to transverse relaxation of ^{15}N spins from chemical exchange processes can be identified unambiguously using the η_{xy}/η_z ratios. When $R_{ex} = 0$ is set, eq 21 can be solved to yield an estimate of the exchange-free transverse relaxation rate, R_2^0, purely due to dipolar and CSA relaxation:

$$R_2^0 = (R_1 - 1.249\sigma_{NH})\frac{\eta_{xy}}{\eta_z} + 1.079\sigma_{NH} \qquad (26)$$

in which η_{xy}/η_z can represent the experimentally determined ratio, or the ratio calculated from the experimentally determined diffusion tensor. The former method does not rely on the assumption that the degree of internal motion is limited. The latter approach has the advantage that, once the diffusion tensor is determined from ^{15}N spins for which η_{xy}/η_z has been determined, R_2^0 can be calculated for ^{15}N spins for which only the auto relaxation rate constants are available. Thus, by comparison with eq 3, the value of the chemical exchange contribution to transverse relaxation is given by

$$R_{ex} = R_2 - R_2^0 \qquad (27)$$

in which R_2 is measured by CPMG[65,66] or $R_{1\rho}$ experiments[24] or calculated from the ^{15}N line width.[14] The functional form of R_{ex} depends on the detailed nature of the exchange process and on the experiment used to measure R_2. The values of $R_2 - R_2^0$ determined using the measured η_{xy}/η_z ratios for *E. coli* RNaseH are plotted as a function of amino acid sequence in Figure 6. Results for one residue, K60, calculated from the predicted η_{xy}/η_z ratio is shown as an open symbol in Figure 6. As shown, only two residues, K60 and W90, exhibit values of $R_{ex} = 7.90 \pm 0.23$ and 2.46 ± 0.53, respectively, that are greater than 1 s^{-1}.

Conventional reduced spectral density mapping using eqs 20 determines $J(0.87\omega_H)$ from σ_{NH}, $J(\omega_N)$ from R_1 and σ_{NH}, and $J(0)$ from R_2, R_1, and σ_{NH}. As a consequence, the values of $J(0)$ are systematically increased for spins subject to chemical exchange which complicates the subsequent interpretations of the spectral density mapping results.[67] Values of $J(0)$ independent of exchange can be calculated from the η_{xy}/η_z ratios, R_1, and σ_{NH} using the following relationship:

$$J(0) = \frac{3}{4}\left[2\frac{\eta_{xy}}{\eta_z} - 1\right]J(\omega_N) \qquad (28)$$

in which $J(\omega_N)$ is obtained from R_1 and σ_{NH} using eqs 20. Figure 7 shows the $J(0)$ values calculated from the η_{xy}/η_z ratios for RNaseH as a function of amino acid sequence.

Discussion

Although dipolar/CSA relaxation interference has long been recognized,[35] new applications of this phenomenon have emerged for measuring chemical shift anisotropies,[26,40,68,69] peptide backbone ψ dihedral angles,[70] and bond vector order parameters.[26,71] Differential relaxation due to the interference

(64) Katayanagi, K.; Miyagawa, M.; Matsushima, M.; Ishikawa, M.; Kanaya, S.; Nakamura, H.; Ikehara, M.; Matsuzaki, T.; Morikawa, K. *J. Mol. Biol.* **1992**, *223*, 1029−1052.
(65) Carr, H. Y.; Purcell, E. M. *Phys. Rev.* **1954**, *94*, 630−638.
(66) Luz, Z.; Meiboom, S. *J. Chem. Phys.* **1963**, *39*, 366−370.
(67) Peng, J. W.; Wagner, G. *J. Magn. Reson.* **1992**, *98*, 308−332.
(68) Tjandra, N.; Bax, A. *J. Am. Chem. Soc.* **1997**, *119*, 9576−9577.
(69) Tjandra, N.; Bax, A. *J. Am. Chem. Soc.* **1997**, *119*, 8076−8082.
(70) Yang, D.; Konrat, R.; Kay, L. E. *J. Am. Chem. Soc.* **1997**, *119*, 11938−11940.
(71) Zeng, L.; Fischer, M. W. F.; Zuiderweg, E. R. P. *J. Biomol. NMR* **1996**, *7*, 157−162.

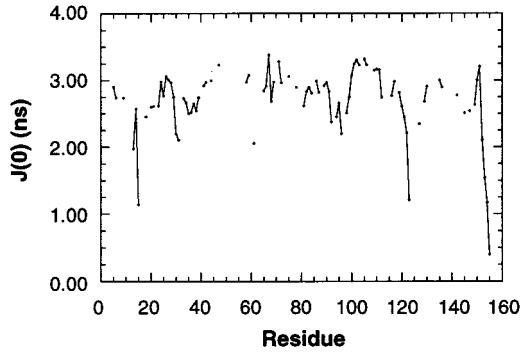

Figure 7. Reduced spectral density mapping. Values of $J(0)$ are plotted versus residue number for RNaseH. The reduced spectral densities $J(\omega_N)$ and $J(0.870\omega_H)$ (not shown) were determined from R_1 and σ_{NH} by the usual approach using eq 20; $J(0)$ was determined from η_{xy}/η_z using eq 28.

effect also has been used to narrow resonance line widths at high static magnetic field strengths.[72]

As demonstrated herein, $^1H-^{15}N$ dipolar/^{15}N CSA relaxation interference also can be used to distinguish the contributions from chemical exchange and rotational diffusion anisotropy to transverse relaxation of ^{15}N spins in biological macromolecules by measuring longitudinal and transverse cross-correlation rate constants, η_z and η_{xy}. The η_{xy} rate constant, which characterizes the cross-relaxation between in-phase and antiphase coherences, is measured using the method of Tjandra et al.[26] A new experiment was developed to measure the former rate constant, which characterizes the cross-relaxation between longitudinal magnetization and two-spin order. Both experiments rely on the simple algebraic form of $\exp(-\mathbf{R}t)$ obtained when the 2×2 relaxation matrix $\mathbf{R}$ is symmetric with identical diagonal elements. In the pulse sequence for measuring η_{xy}, shown in Figure 1a, the diagonal elements of the transverse relaxation matrix, R_2 and R_{2IS}, are averaged by evolution under the $^1H-^{15}N$ scalar coupling Hamiltonian during the relaxation period τ, provided that τ is an integral multiple of $1/J$. The operators S_z and $2I_zS_z$ commute with the scalar coupling Hamiltonian; therefore, in the pulse sequence for measuring η_z, shown in Figure 1b, the diagonal elements of the longitudinal relaxation rate matrix, R_1 and R_{1IS}, are averaged during the relaxation period τ by pulse sequence elements that periodically exchange the magnitudes of the S_z and $2I_zS_z$ spin orders. The averaging procedure is exact to second order in τ, and numerical calculations shown in Figure 2 indicate that the resulting effective evolution during the relaxation period closely approximates the ideal behavior for times up to $\sim 3/(R_1 + R_{1IS})$.

Under the assumption that the angle between the symmetry axis of the (approximately) axially symmetric ^{15}N CSA tensor and the N−H bond vector is small ($<20°$),[28−30] the η_{xy}/η_z ratio is independent of the magnitude of the CSA and dipolar interactions and depends only on the spectral density functions, $J(0)$ and $J(\omega_N)$. In contrast to the R_2/R_1 ratio, η_{xy}/η_z is independent of chemical exchange contributions to transverse relaxation, because a chemical kinetic process merely exchanges a spin between magnetic environments and does not induce coherence transfer between S_y and $2I_zS_y$ operators or between S_z and $2I_zS_z$ operators. Of course, η_{xy} and η_z represent the population-weighted average rate constants if the ^{15}N spin exchanges between environments with significantly different CSA tensors. The accuracy of the methods adopted to measure the parameters η_{xy}, and η_z was verified by comparing the η_{xy}/η_z ratios to the $(R_2 - 1.079\sigma_{NH})/(R_1 - 1.249\sigma_{NH})$ ratios, as shown in Figure 4.

Measurement of η_{xy}/η_z has two main purposes. First, for sites with limited internal mobility, the ratio is independent of contributions from internal motion to the spectral density function. Accordingly, the observed variations in η_{xy}/η_z can be used to determine the rotational diffusion tensor of a biological macromolecule using eqs 22−25. Second, η_{xy}/η_z, R_1, and σ_{NH} can be used to calculate the transverse relaxation rate constant, R_2^0, due solely to the dipolar and CSA relaxation mechanisms using eq 26. This result can be used to measure the chemical exchange contribution to R_2 using eq 27 or to determine a value of $J(0)$ from eq 28 that does not contain systematic contributions from chemical exchange.

In a previous report on the dynamics of RNaseH at 285, 300, and 310 K, the rotational diffusion tensor for RNaseH was determined by analysis of R_2/R_1 ratios.[34] To avoid including data for residues subject to conformational exchange, residues with R_2/R_1 ratios more than one standard deviation smaller or larger than the mean ratio were excluded from the analysis. In addition, to provide internal consistency, only residues for which data were available at all three temperatures were included in the analysis. The R_2/R_1 ratios for 37 backbone ^{15}N spins were described by an axially symmetric diffusion tensor with $D_\parallel/D_\perp = 1.12 \pm 0.02$. The major advantage of the η_{xy}/η_z ratios in determining the diffusion tensor is that only small ratios, reflecting extensive internal motions on picosecond to nanosecond time scales, must be excluded from the analysis. In contrast to the analysis of R_2/R_1 ratios, no decisions must be made as to whether to include or exclude large η_{xy}/η_z ratios. As a result, data for 70 ^{15}N spins were included in the analysis of the diffusion tensor in the present work. This analysis yielded a significantly higher diffusion anisotropy of $D_\parallel/D_\perp = 1.23 \pm 0.04$. Most importantly, a number of residues in helix α_D, such as V101 and L111, which have R_2/R_1 ratios >8.20, compared with a mean of 7.05 in RNaseH, were excluded from the earlier analysis but have equally large η_{xy}/η_z ratios; this observation immediately indicates that the increased values of R_2/R_1 reflect rotational diffusion anisotropy rather than chemical exchange effects. The N−H bond vectors for these residues are aligned almost collinearly with the unique axis of the diffusion tensor. Consequently, these residues are particularly important in determining the anisotropy of the diffusion tensor because a preponderance of the data are for residues for which the N−H bond vectors are oriented at angles $>54.7°$ relative to the unique axis of the diffusion tensor.[20]

Because the η_{xy}/η_z ratios clearly distinguish between residues for which the R_2/R_1 ratios are elevated due to rotational anisotropy rather than exchange, the set of R_2/R_1 ratios can be expanded to include data previously excluded or the η_{xy}/η_z and R_2/R_1 ratios can be analyzed simultaneously. The local diffusion approach is particularly convenient for analysis of data derived from independent experiments, because the calculation of the local diffusion constants, which depends on the nature of the spin relaxation experiment, is formally separate from the calculation of the diffusion tensor.[20] The results of the simultaneous analysis of 70 η_{xy}/η_z and 70 R_2/R_1 ratios yields a value of $D_\parallel/D_\perp = 1.25 \pm 0.03$ for RNaseH using the 1rnh structural coordinates. The unique axis of the diffusion tensor for the analysis of the η_{xy}/η_z ratios alone and for the simultaneous analysis of η_{xy}/η_z and R_2/R_1 are oriented within 4.2° of each other. This result further indicates the quantitative accuracy of

(72) Pervushin, K.; Riek, R.; Wider, G.; Wüthrich, K. *Proc. Natl. Acad. Sci. U.S.A.* **1997**, *94*, 12366−12371.

the η_{xy}/η_z ratios measured by the experimental methods presented in this work.

In principle, particularly for multiple domain proteins or biological macromolecular complexes, the orientational information contained in the values η_{xy}/η_z can be used as structural constraints in the refinement of a protein or nucleic acid structures, as has been done for R_2/R_1 ratios.[18,73] Again, the absence of chemical exchange contributions to η_{xy}/η_z provides additional robustness in such refinements.

Comparison between the cross-correlation and auto relaxation rates allows for the determination of chemical exchange contributions to the R_2 by using eqs 26 and 27. As shown in Figure 6, K60 and W90 are the only residues exhibiting an apparent chemical exchange effect greater than 1 s^{-1}. The value of R_{ex} for W90 obtained in this study, 2.5 $\pm$ 0.2 s^{-1}, agrees well with the value of 2.3 $\pm$ 0.3 s^{-1} obtained by fitting the model-free formalism to ^{15}N R_1, R_2, and σ_{NH} data.[34] Results for K60 have not been obtained previously from data acquired at 300 K due to resonance overlap with I7. Data acquired at 285 and 310 K, however, confirm that this residue is subject to large chemical exchange effects comparable to the results obtained here.[34] The reduced amide ^1H line widths for deuterated RNaseH increases the resolution of the NMR spectra and permits quantification of the laboratory frame relaxation rate constants for K60. Nevertheless, remaining overlap between the resonances for I7 and K60 still may lead to an underestimation of exchange effects by partially averaging the relaxation rate constants of the two ^{15}N spins. A number of residues show apparent R_{ex} values of approximately 1 s^{-1} in Figure 6. Which of these reflect small chemical exchange effects cannot be established definitively from the present data. The value obtained for K91 of 0.8 $\pm$ 0.3 s^{-1} is somewhat smaller than the value of 1.5 $\pm$ 0.2 s^{-1} obtained from the model-free formalism.[34] However, the temperature dependence of R_{ex} observed for K91 is very similar to the temperature dependence observed for W90 which supports the identification of an exchange contribution to relaxation of K91.[34] Most importantly, the R_2/R_1 ratio for W90 (8.62 $\pm$ 0.15) is not significantly larger than the ratio observed for residues such as V101 (8.62 $\pm$ 0.08). However, the η_{xy}/η_z ratios clearly identify significant chemical exchange contributions to relaxation of W90 while the increased R_2/R_1 ratios for V101 result from rotational diffusion anisotropy (vide supra). Thus, the use of η_{xy}/η_z ratios to identify chemical exchange avoids the systematic misattribution of exchange effects based on the distribution of observed R_2 values.

As discussed in the Introduction, chemical exchange effects can be recognized from the dependence of the apparent transverse relaxation rate constant on the amplitude of either the static magnetic field in the laboratory frame[4,6,23] or on the effective field in the rotating reference frame.[12−14,25] In both of these analyses, the contribution to transverse relaxation arising from dipolar and CSA interactions must be separated from the chemical exchange effects by curve-fitting. This contribution can be obtained independently from the η_{xy}/η_z ratios using eq 26 and used to reduce the number of free parameters to be determined from the field-dependent relaxation data and increase the precision of the exchange parameters obtained.

(73) Tjandra, N.; Garrett, D. S.; Gronenborn, A. M.; Bax, A.; Clore, G. M. *Nat. Struct. Biol.* **1997**, *4*, 443−449.

Conclusion

The method we have developed for measuring the ratio between the transverse and longitudinal cross-relaxation rate constants resulting from $^1H-^{15}N$ dipole and ^{15}N CSA relaxation interference provides unambiguous identification of chemical exchange contributions to transverse relaxation. This method also permits the rotational diffusion anisotropy of biological macromolecules to be determined more accurately by eliminating confounding effects of chemical exchange. Knowledge of the principal values of the CSA tensor is not required in the interpretation of this experiment, provided that the orientations of the CSA and dipole−dipole tensors do not differ greatly. Separating contributions from chemical exchange processes to transverse relaxation has posed a significant problem in the interpretation of ^{15}N spin relaxation data in biological macromolecules for many years.[11] The problem recently has become more acute as the effects of rotational diffusion anisotropy on ^{15}N spin relaxation have become better appreciated.[16,18,22] Existing methods for identifying chemical exchange rely on the quadratic dependence of the exchange line broadening on the magnitude of either the static magnetic field[4,6,23] or the effective field in the rotating frame.[12−14,25] The former requires access to a wide range of high-field NMR spectrometers, and the latter is a specialized technique employing high-power spin-locking radio frequency fields and lengthy experimental acquisition times. This new approach uses data acquired at a single static magnetic field and is no more difficult than conventional laboratory reference frame relaxation experiments. By solving the conundrum presented by deconvolution of chemical exchange contributions to transverse relaxation, the experiments proposed in this paper will be widely applicable to studies of the dynamic properties of proteins and other biological macromolecules.

Acknowledgment. We thank Mikael Akke (Lund University), Ann McDermott (Columbia University), and Clay Bracken (Columbia University) for many helpful discussions. This work was supported by NIH Training Grant 2 T32 GM 08281 (C.D.K.), NIH postdoctoral NSRA 1 F32 GM 19247 (J.P.L.), NIH grant GM 40089 (M.R.), and NIH grant GM 50291 (A.G.P.).

Supporting Information Available: One table containing measured values of η_{xy}, η_z, R_2, R_1, and σ_{NH} for 91 ^{15}N spins in $^2H/^{15}N$-labeled *E. coli* ribonuclease H (3 pages, print/PDF). See any current masthead page for ordering information and Web access instructions.

JA980832L